

Focused electromagnetic doughnut pulses and their interaction with interfaces and nanostructures

Tim Raybould,^{1,*} Vassili Fedotov,¹ Nikitas Papisimakis,¹ Ian Youngs,²
and Nikolay Zheludev^{1,3}

¹*Optoelectronics Research Centre & Centre for Photonic Metamaterials, University of Southampton, UK*

²*DSTL, Salisbury, UK*

³*Centre for Disruptive Photonic Technologies, TPI, Nanyang Technological University, Singapore*

[*T.A.Raybould@soton.ac.uk](mailto:T.A.Raybould@soton.ac.uk)

Abstract: The “focused doughnut,” a single-cycle electromagnetic perturbation of toroidal topology with inseparable time and spatial dependencies propagates at the speed of light in vacuum, as was shown by Hellwarth and Nouchi in 1996. While normal incidence reflection and refraction of conventional electromagnetic pulses in isotropic media do not lead to polarization changes, “focused doughnut” pulses undergo complex field transformations owing to the toroidal field structure and the presence of longitudinal components. We also demonstrate that “focused doughnuts” can interact strongly with structured media exciting dominant dynamic toroidal dipoles in spherical dielectric particles.

© 2016 Optical Society of America

OCIS codes: (320.5550) Pulses; (260.2110) Electromagnetic optics; (290.5850) Scattering, particles; (350.5500) Propagation.

References and links

1. J. D. Jackson, *Classical Electrodynamics* (John Wiley & Sons, Inc, 1998).
2. J. Brittingham, “Focus waves modes in homogeneous Maxwell’s equations: Transverse electric mode,” *J. Appl. Phys.* **54**(3), 1179–1189 (1983).
3. T. T. Wu and R. W. P. King, “Comment on “Focus wave modes in homogeneous Maxwell’s equations: Transverse electric mode,”” *J. Appl. Phys.* **56**(9), 2587–2588 (1984).
4. P. Bélanger, “Packetlike solutions of the homogeneous-wave equation,” *J. Opt. Soc. Am. A* **1**(7), 723–724 (1984).
5. A. Sezginer, “A general formulation of focus wave modes,” *J. Appl. Phys.* **57**(3), 678–683 (1985).
6. R. W. Ziolkowski, “Exact solutions of the wave equation with complex source locations,” *J. Math. Phys.* **26**(4), 861–863 (1985).
7. R. W. Ziolkowski, “Localized transmission of electromagnetic energy,” *Phys. Rev. A* **39**(4), 2005–2033 (1989).
8. J. Lekner, “Localized electromagnetic pulses with azimuthal dependence,” *J. Opt. A: Pure Appl. Opt.* **6**(7), 711–716 (2004).
9. J. Lekner, “Helical light pulses,” *J. Opt. A: Pure Appl. Opt.* **6**(10), 29–32 (2004).
10. S. Feng, H. G. Winful and R. W. Hellwarth, “Gouy shift and temporal reshaping of focused single-cycle electromagnetic pulses,” *Opt. Lett.* **23**(14), 385–387 (1998).
11. S. Feng, H. G. Winful and R. W. Hellwarth, “Spatiotemporal evolution of single-cycle electromagnetic pulses,” *Phys. Rev. E* **59**(4), 4630–4649 (1999).
12. S. Hunsche, S. Feng, H. G. Winful, A. Leitenstorfer, M. C. Nuss and E. P. Ippen, “Spatiotemporal focusing of single-cycle light pulses,” *J. Opt. Soc. Am. A* **16**(8), 2025–2028 (1999).
13. R. W. Hellwarth and P. Nouchi, “Focused one-cycle electromagnetic pulses,” *Phys. Rev. E* **54**(1), 889–895 (1996).
14. X. Gu, S. Akturk and R. Trebino, “Spatial chirp in ultrafast optics,” *Opt. Commun.* **242**(4), 599–604 (2004).

15. A. M. Shaarawi, I. M. Besieris and R. W. Ziolkowski, "Localized energy pulse trains launched from an open, semi-infinite, circular waveguide," *J. Appl. Phys.* **65**(2), 805–813 (1989).
16. R. W. Ziolkowski, "Properties of electromagnetic beams generated by ultra-wide bandwidth pulse-driven arrays," *IEEE Trans. Antennas Propag.* **40**(8), 888–905 (1992).
17. C. Varin, M. Piché and M. A. Porras, "Acceleration of electrons from rest to GeV energies by ultrashort transverse magnetic laser pulses in free space," *Phys. Rev. E* **71**(2), 026603 (2005).
18. I. J. Youngs, N. Bowler, K. P. Lymer and N. Hussain, "Dielectric relaxation in metal-coated particles: the dramatic role of nano-scale coatings," *J. Phys. D: Appl. Phys.* **38**, 188 (2005).
19. I. J. Youngs, N. Bowler and O. Ugurlu, "Dielectric relaxation in composites containing electrically isolated particles with thin semi-continuous metal coatings," *J. Phys. D: Appl. Phys.* **39**, 1312 (2006).
20. C. Vrejoiu, "Electromagnetic multipoles in cartesian coordinates," *J. Phys. A* **35**(46), 9911–9922 (2002).
21. E. E. Radescu and G. Vaman, "Exact calculation of the angular momentum loss, recoil force, and radiation intensity for an arbitrary source in terms of electric, magnetic, and toroid multipoles," *Phys. Rev. E.* **65**(4), 046609 (2002).
22. T. Kaelberer, V. A. Fedotov, N. Papasimakis, D. P. Tsai and N. I. Zheludev, "Toroidal dipolar response in a metamaterial," *Sci. Rep.* **3**(6010), 1510–1512 (2010).
23. V. A. Fedotov, A. V. Rogacheva, V. Savinov, D. P. Tsai and N. I. Zheludev, "Resonant transparency and non-trivial non-radiating excitations in toroidal metamaterials.1," *Science* **3**, 2967 (2013).
24. A. A. Basharin, M. Kafesaki, E. N. Economou, C. M. Soukoulis, V. A. Fedotov, V. Savinov and N. I. Zheludev, "Dielectric Metamaterials with Toroidal Dipolar Response," *Phys. Rev. X* **5**(1), 011036 (2015).

1. Introduction

The homogeneous Maxwell's equations describe the behavior of electromagnetic radiation in free space. Infinite energy plane waves of the form $Ae^{i(kr-\omega t)}$ are the most well established solutions and are used extensively in the geometric optics regime [1]. However, pulse solutions to the homogeneous Maxwell's equations i.e. representing localised propagation of finite electromagnetic energy, are significantly less well analyzed. A first attempt to produce a mathematical formulation for three dimensional, non-dispersive, source-free solutions to homogeneous Maxwell's equations yielded the *focused wave mode* (FWM) solutions, suggesting the possibility for efficient transport of electromagnetic energy in free-space [2]. FWMs were required to meet six criteria: 1) satisfy the homogeneous Maxwell's equations, 2) be continuous and non-singular, 3) have a three-dimensional pulse structure, 4) be non-dispersive for all time, 5) move at light velocity c along straight lines, and 6) carry finite electromagnetic energy. Although the original FWMs were subsequently shown to violate the sixth criterion [3–5], the finite energy requirement was satisfied by utilizing superpositions of the FWMs over carefully chosen weighting functions [6, 7]. These superpositions are termed as *electromagnetic directed energy pulse trains* (EDEPTs) and can be tailored so as to give localized propagation of electromagnetic energy in space and time. A wide variety of pulses have been established within the EDEPT family, including the modified power spectrum pulse [7], pulses with azimuthal dependence [8, 9], "focused pancake" pulses [10–12], and the "*focused doughnut*" (FD) pulse [13]. The FD pulse is of particular interest owing to its complex toroidal field geometry, space-time non-separability, and polynomial localization of energy. Finally, as a free-space toroidal electromagnetic perturbation, investigation of the FD pulse complements the burgeoning field of toroidal electrodynamics in matter.

In this letter we give a detailed description of the propagation properties of FD pulses and their interactions with matter. We demonstrate that due to the toroidal field configuration of the FD pulses, even reflection from dielectric and metallic interfaces can lead to complex field transformations. We show that dielectric nanoparticles under illumination with FD pulses exhibit broadband, multi-mode excitations, with a pronounced toroidal dipole component. The paper is organized as follows. Section 2 introduces the theoretical formalism for the description of FD pulses. Studies in the transient domain are considered and these numerical models are used as a basis for examining the interaction of FD pulses with matter. Section 3 examines the transformation of the FD field topologies when the pulse is incident on dielectric-dielectric

and dielectric-metal interfaces, and Section 4 considers the interaction of FD pulses with non-dispersive, dielectric nanoparticles.

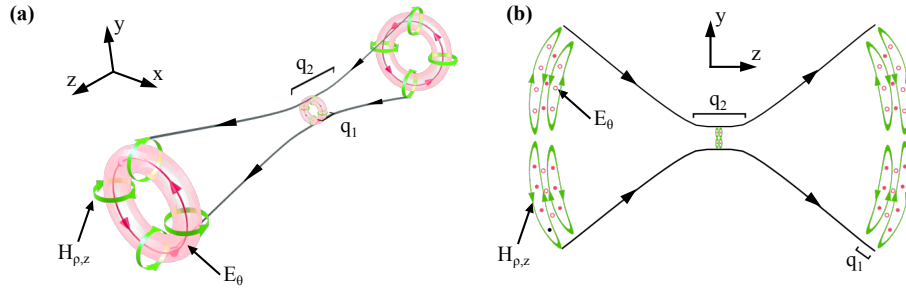


Fig. 1. Field topology and focusing properties of the transverse electric “focused doughnut” pulse. The electric E and magnetic H fields are represented by green and red arrows respectively. The effective wavelength parameter q_1 and the pulse focal region depth q_2 are indicated on both diagrams, along with the region of maximum energy concentration at $z = 0, t = 0$. The evolution of the pulse envelope is indicated by the black lines and arrows.

2. The “focused doughnut” pulse

The FD pulse was first established as a solution to the homogeneous Maxwell’s equations by Hellwarth and Nouchi [13]. As space-time non-separable solutions to Maxwell’s equations, FD pulses can be classified in transverse electric (TE) and transverse magnetic (TM) field configurations, with the electric and magnetic fields for the TE case given in cylindrical coordinates (ρ, θ, z) as:

$$E_\theta = -4if_0 \sqrt{\frac{\mu_0}{\epsilon_0}} \frac{\rho (q_1 + q_2 - 2ict)}{[\rho^2 + (q_1 + i\tau)(q_2 - i\sigma)]^3} \quad (1)$$

$$H_\rho = 4if_0 \frac{\rho (q_2 - q_1 - 2iz)}{[\rho^2 + (q_1 + i\tau)(q_2 - i\sigma)]^3} \quad (2)$$

$$H_z = -4f_0 \frac{\rho^2 - (q_1 + i\tau)(q_2 - i\sigma)}{[\rho^2 + (q_1 + i\tau)(q_2 - i\sigma)]^3} \quad (3)$$

where $\sigma = z + ct$, $\tau = z - ct$ and f_0 is an arbitrary normalisation constant. The parameters q_1 and q_2 have the dimensions of length and represent respectively the effective wavelength of the pulse and the focal region depth. Beyond the focal region ($|z| > q_2$), the FD diffracts in the same manner as a Gaussian pulse with wavelength q_1 and Rayleigh length q_2 . The name of this pulse is derived from its three-dimensional field topology, which is illustrated in Fig. 1(a) and (b). The azimuthal electric field in Eq. (1) forms closed loops that are zero valued on axis. The magnetic field components [Eqs. (2) and (3)] form closed loops around the electric field, forming the meridians of a torus structure. The field along the meridians of the torus results in strong longitudinal field component on axis due to the increase in field density within the centre of the torus. The TM solutions are readily obtained by interchanging electric and magnetic field components. Further separating the real and imaginary parts of Eqs. (1)-(3) yields two families of pulses, corresponding to a single cycle and $1\frac{1}{2}$ cycle pulse respectively.

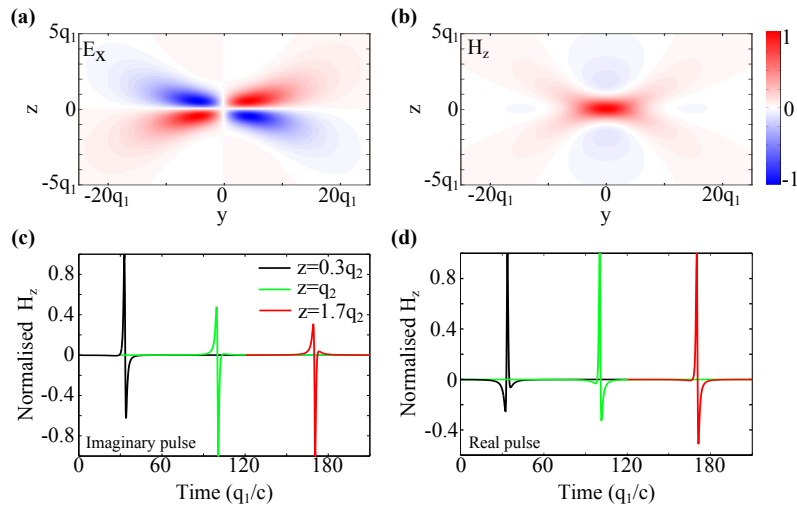


Fig. 2. Spatial and temporal structure of the “focused doughnut” pulses. Panels (a) and (b) show respectively the normalized transverse electric and longitudinal magnetic fields along a yz cross-section at time $t = 0$. The characteristic parameters of the FD pulse in all cases are $q_2 = 100q_1$. All plots are generated from the analytical form of the FD pulse, Eqs. (1-3). The propagation properties of the TM pulse are identical to the TE case presented here, by replacing electric (magnetic) with magnetic (electric) fields. (c) and (d) show the evolution of the on-axis field component of both the real and imaginary pulses respectively as they propagate, demonstrating the transformations between the single and $1\frac{1}{2}$ cycle pulses.

Eqs. (1)-(3) are plotted out explicitly in Fig. 2(a) and (b) along a yz cross-section, showing explicitly the transverse electric field and longitudinal magnetic field at a time $t = 0$. The few cycle nature of the pulse is evident, with Fig. 2(a) showing a single cycle of the transverse electric field and Fig. 2(b) showing the corresponding $1\frac{1}{2}$ cycle longitudinal magnetic field. As expected, the longitudinal field component of FD pulses is the only component that is non-zero at $\rho = 0$. The energy density ($\mu_0 H^2 + \epsilon_0 E^2$) drops off polynomially with r ($r = \sqrt{\rho^2 + z^2}$), decaying as r^{-8} (for the real pulse) and r^{-10} (for the imaginary pulse) at the point of maximum focus ($z = 0, t = 0$). Both real and imaginary FD solutions have been shown to possess equal and finite total energy [13].

It is worth noting that whilst the original paper by Hellwarth and Nouchi categorised the two families of FD into single (imaginary) and $1\frac{1}{2}$ cycle (real) pulses, significant temporal reshaping of the pulses occurs as they propagate along z . This is emphasised in Fig. 2(c) and (d) which shows the spatio-temporal transformations that both the real and imaginary pulses undergo as they propagate along z . It is immediately clear from Fig. 2(c) that as the pulses propagate beyond the q_2 parameter, the imaginary pulse evolves from single cycle to $1\frac{1}{2}$ cycles, whilst the real pulse evolves from $1\frac{1}{2}$ cycle to single cycle. Similar transformations have been described for other pulses in the EDEPT family and experimentally for single-cycle Gaussian Terahertz pulses, and they have been explained in terms of the Gouy phase shift of the pulses [10, 12].

As a result of their short cycle nature, FD pulses are considered to be ultra-broad bandwidth pulses. Hellwarth and Nouchi give a far-field ($z \gg q_2$) approximation for the Fourier spectra of a real FD in their original paper:

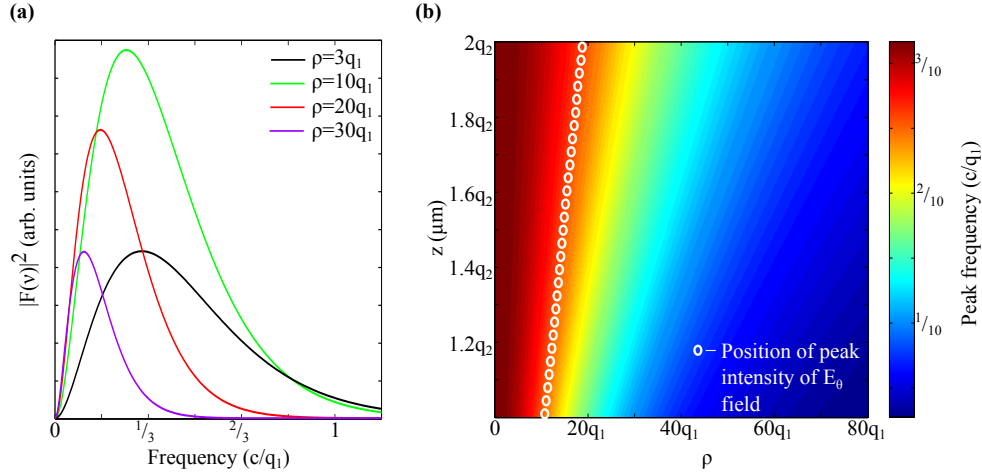


Fig. 3. Fourier spectrum of the real FD pulses. (a) shows the intensity of the Fourier spectrum for $q_2 = 100q_1$ at $z = q_2$ and for four different radial positions ρ . (b) shows the evolution of the peak frequency as a function of ρ and z for $z = q_2 \rightarrow 2q_2$.

$$F'_\omega = \left(\frac{i\pi\mu_0 f_0 \omega |\omega| \sin\varphi}{2rc^2} \right) e^{\frac{i\omega r - |\omega|Q}{c}} \quad (4)$$

where $Q = [q_1 + q_2 - (q_2 - q_1)\cos\varphi]/2$ and φ is the polar angle. The equivalent Fourier spectrum for the imaginary pulse is formed by $F''_\omega = (i\omega/|\omega|)F'_\omega$.

A number of intriguing properties of the FD pulse can be inferred from the Fourier decomposition. The dependence of the Fourier spectrum on ρ is emphasised in Fig. 3(a) which plots the intensity of the Fourier spectrum at four different values of ρ . It can be seen that high frequency components dominate the centre of the FD and lower frequency components become prevalent as ρ increases. This effect can be visualised by considering Fig. 2(a), where the curvature of the pulse wavefronts indicates a change in frequency as ρ increases. The evolution of the peak frequency as a function of both ρ and z is shown in Fig. 3(b) over a propagation distance of q_2 from $z = q_2 \rightarrow 2q_2$. It can be seen that, as the FD evolves in space, different radial points acquire different peak frequencies. However, it can be noted from the white circles in Fig. 3(b) that, as the pulse propagates, the peak frequency at the point of peak intensity remains constant, in this case, at the value of $\sim \frac{c}{4q_1}$.

The property of a varying peak frequency transverse to the pulse propagation direction is known as spatial chirp, and is a common occurrence in ultrafast optics. However, whilst the spatial chirp of the FD is intrinsic to the pulse, it generally arises in ultrafast optics due to misalignment of optical elements used for production of ultrashort pulses e.g. prisms, tilted substrates and Fourier pulse shapers [14]. This lack of control of the phenomenon leads to the spatial chirp being considered an undesirable side-effect. The well-defined spatial chirp of the FD pulse however, allows to exploit this property by coupling frequency information to spatial positions of the pulse, a situation which is of interest for spectroscopy for example. In addition, it can be noted that the spatial chirp of the FD is axially symmetric, as per the topology of the pulse, and so can in fact be termed radial chirp.

A further point is that for all ρ , the bandwidth of the FD pulse is greater than the peak frequency. Consider for instance the Fourier spectrum at $\rho = 10q_1$ [Fig. 3(a), green curve]. The

peak frequency ν_0 at this ρ value is $\frac{c}{4q_1}$, compared to a full width at half maximum bandwidth of $\sim 1.1\nu_0$. This can be taken in contrast to the typical bandwidth-limited pulses produced by solid-state lasers, for which the bandwidth will always be smaller than the peak frequency.

To date, there has not been an experimental realisation of the FD pulse. Although waveguides [15] and ultra-wide bandwidth antenna arrays [16] have been suggested as potential generating platforms for localised pulses, the creation of an FD pulse remains a non-trivial task, owing to the need for simultaneous control of spatial and temporal dispersion over a wide bandwidth. Despite this, the nature of the FD pulses has resulted in several potential applications being suggested. The strongly localised nature of the pulse for $|z| < q_2$ could be exploited in microscopy, communications and directed energy transfer [13]. The presence of the longitudinal field component was discussed in detail by Hellwarth and Nouchi in terms of a mechanism for accelerating co-propagating particles, and later by Varin et al. [17].

3. Interaction with plane interfaces

Although the properties of the FD pulse in free-space have been well established, and the propagation dynamics and reshaping of similar pulses have been described in the literature, there has been a very limited treatment of the interaction of such complex pulses with matter. In general, the problem is not amenable to analytical considerations. To this end, we employ a commercial finite element solver to evaluate the interactions of the FD pulse with continuous matter. In this section, we give the first explicit analysis of the transformations of the FD field components under reflection and transmission when incident on semi-infinite dielectrics and *perfect electric conductor* (PEC) boundaries.

We first consider a PEC boundary located at $z = 20q_1$ in the free-space propagation domain. Figure 4(a) and (b) show the TE and TM pulse respectively at two times – one prior to incidence on the boundary (t_1) and one after the pulse has been reflected (t_2).

For the TE FD pulse in Fig. 4(a), the transverse electric and longitudinal magnetic field components are shown. It is clear from examining the field distributions at the two time steps that, upon reflection, the transverse electric field of the TE pulse rotates in the same direction with respect to the propagation direction as before reflection. Similarly, the longitudinal magnetic field component both before and after reflection has a component parallel to the propagation direction leading the pulse.

In contrast however, the reflection of the TM pulse at the boundary in Fig. 4(b) results in the reversal of both the electric and magnetic field components. After reflection, the transverse magnetic fields are counter-rotating with respect to the propagation direction. The longitudinal electric field component is dominated by a strong component parallel to the propagation direction at the pulse front. Upon reflection, the electric field at the pulse front is anti-parallel to the propagation of the pulse. The presence of a longitudinal field component, anti-parallel to the propagation direction, at the leading edge of the pulse is a particularly intriguing and non-intuitive property of the reflected TM FD pulse.

This modelling of the FD pulse also highlights the spatio-temporal transformations the pulse undergoes, as described in Section 2 and Fig. 2(c) and (d). It can be clearly seen in Fig. 4(a) how, after reflection at the boundary, the transverse magnetic field of the pulse is beginning to transform from single cycle to $1\frac{1}{2}$ cycle nature. Equivalently, the longitudinal electric field is beginning to transform from $1\frac{1}{2}$ cycle to single cycle nature. This transformation is also evident in Fig. 4(b) for the TE pulse.

We now consider interaction at the interface between two dielectric media. The modelling space is separated into two regions – one free space and one of refractive index $n = 2$, with the interface located at $z = 15q_1$ so as to illustrate both the reflected and transmitted pulse. Figure 5 shows the results of these models for both TE and TM FD pulses, with the transverse and

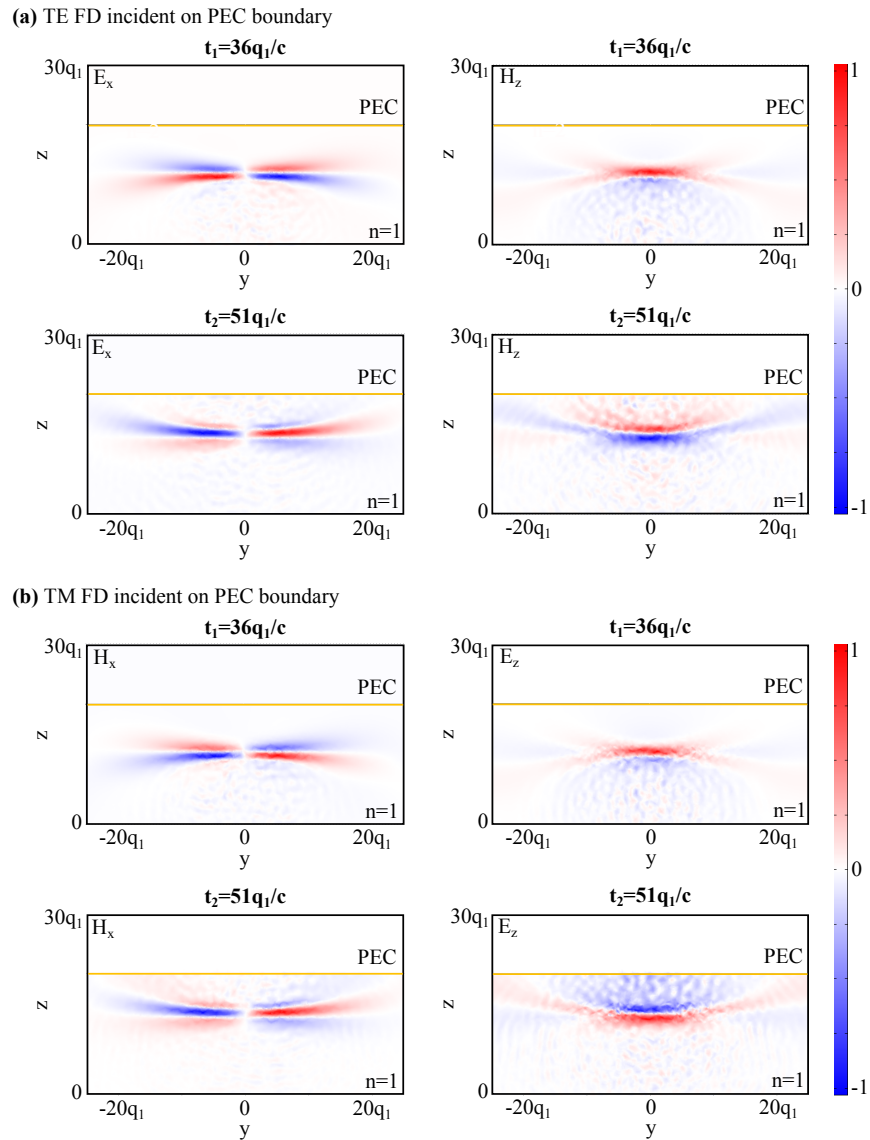


Fig. 4. Reflection of “focused doughnut” pulses from a perfect conductor. (a) Transverse electric (left) and longitudinal (right) magnetic field components of a transverse electric FD pulse before (t_1) and after (t_2) reflection. (b) Similar to (a) but for a transverse magnetic pulse. In both cases the parameters of the FD pulse are $q_2 = 100q_1$ and the boundary is located at a distance $z = 20q_1$ from the focal point of the pulse ($z = 0$). All field components have been normalized to their maximum value.

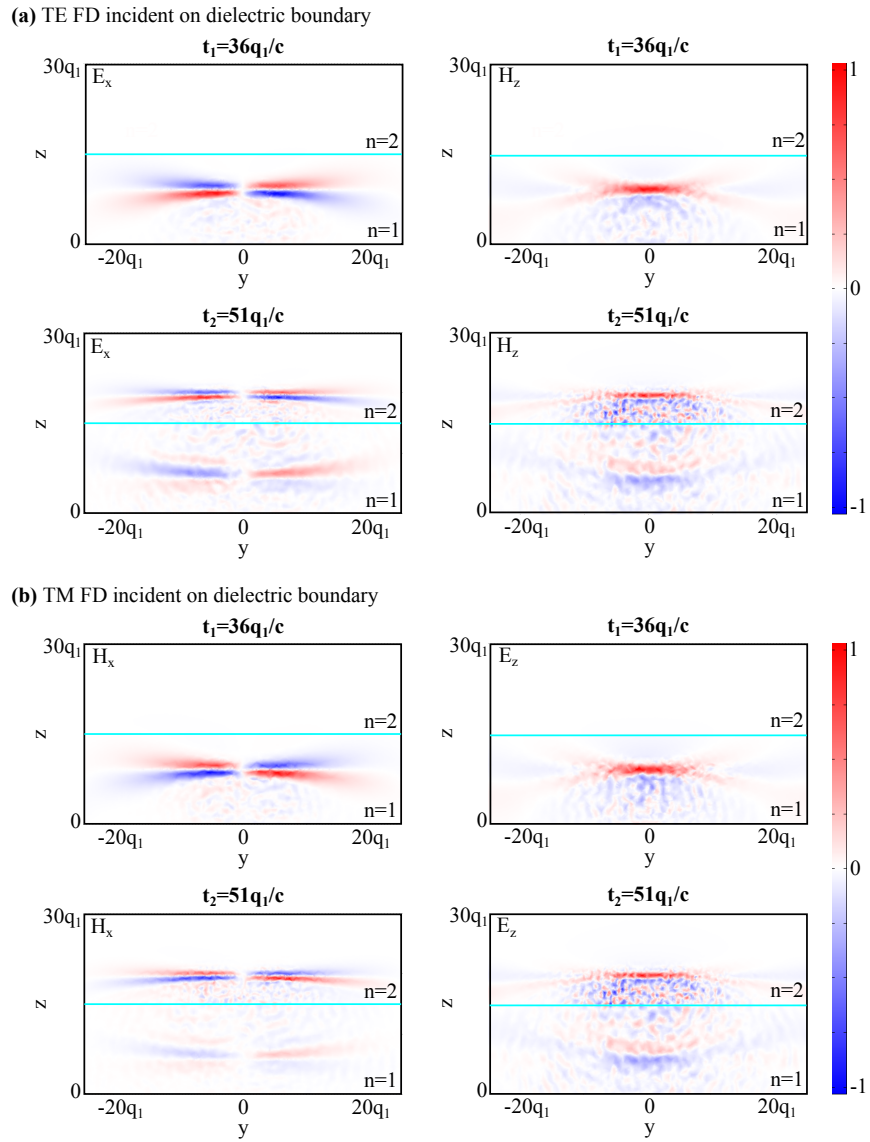


Fig. 5. Reflection and refraction of “focused doughnut” pulses at a vacuum-dielectric interface. (a) Transverse electric (left) and longitudinal magnetic field (right) components of a transverse electric FD pulse before (t_1) and after (t_2) incidence on the interface. (b) Similar to (a) but for a transverse magnetic pulse. In both cases the parameters of the FD pulse are $q_2 = 100q_1$ and the boundary is located at a distance $z = 15q_1$ from the focal point of the pulse ($z = 0$). All field components have been normalized to their maximum value. The dielectric is considered to be semi-infinite with a refractive index $n = 2$.

longitudinal fields shown at two times – one prior to incidence on the boundary (t_1) and one after the pulse has been reflected and transmitted (t_2). In both polarisation cases the toroidal topology of the pulse is maintained after being transmitted through the dielectric interface and it undergoes the expected increase in momentum within the medium as for conventional electromagnetic pulses. Similarly the reflected pulse also maintains its toroidal topology. Evaluation of transmission and reflection coefficients for the reflected and transmitted pulses indicates that both TE and TM FD pulses interact with the semi-infinite dielectric as predicted by the Fresnel equations.

It is worth noting that all models in this section utilise idealised non-dispersive metals and dielectrics, in the form of PEC and a dielectric refractive index of $n = 2$. As illustrated previously in this paper, the FD pulse is highly broadband with a bandwidth greater than the peak frequency. For realistic materials, it is likely that dispersive effects would be present over such a wide frequency range, inducing some reshaping to the temporal profile of the pulse. However, it is expected that this will not limit the analysis of the reflected and transmitted geometries. It could also be considered that this would be a valid description for an FD pulse in the microwave regime, in which metals can generally be approximated as PEC for thicknesses greater than μm -scale [18, 19].

4. Interaction with nanoparticles

The space-time non-separable and ultra-broadband nature of the FD pulses is expected to manifest in an interesting manner when considering their interaction with dielectric nanoparticles. The case considered is that of a spherical nanoparticle located at $\rho = z = 0$. The radius of the nanoparticle is given as q_1 , such that it is less than the width of the FD pulse. In this regime, excitation by the ultra-broadband FD pulse can be expected to excite multiple Mie modes of the dielectric nanoparticle. As in the previous section, the dielectric is given a non-dispersive refractive index of $n = 2$. For an incident TM FD pulse, the interaction with the nanoparticle is dominated by the longitudinal electric field on axis. Figure 6 shows both the simulated interactions [Fig. 6(a) and (b)] and artistic schematics [Fig. 6(c) and (d) insets] for both TE and TM cases.

We first evaluate the normalised electric field intensity within the nanoparticle as a function of frequency. These are shown in Fig. 6(c) and (d) for the TE and TM incidence case respectively. For TE FD incidence, a clear series of Mie modes are excited corresponding to resonant distributions of the azimuthal field throughout the nanoparticle. This is emphasised in Fig. 6(e), which shows out-of-plane electric field distributions for a cross-section through the nanoparticle at three different peaks. In contrast, the spectrum for excitation of the nanoparticle by a TM pulse is more complicated, owing to the interplay between the radial and longitudinal electric field components. As such, the TM excitations are considerably weaker than those from TE pulse incidence. Modes corresponding to distributions of x -aligned (in-plane) E field from three frequencies are shown in Fig. 6(f), corresponding to a series of Mie resonances, similar to the TE pulse case.

To extend this description of FD-nanoparticle interaction, we evaluate the scattering from the microscopic multipole modes excited within the nanoparticle. These are given up to quadrupole order by [20, 21]:

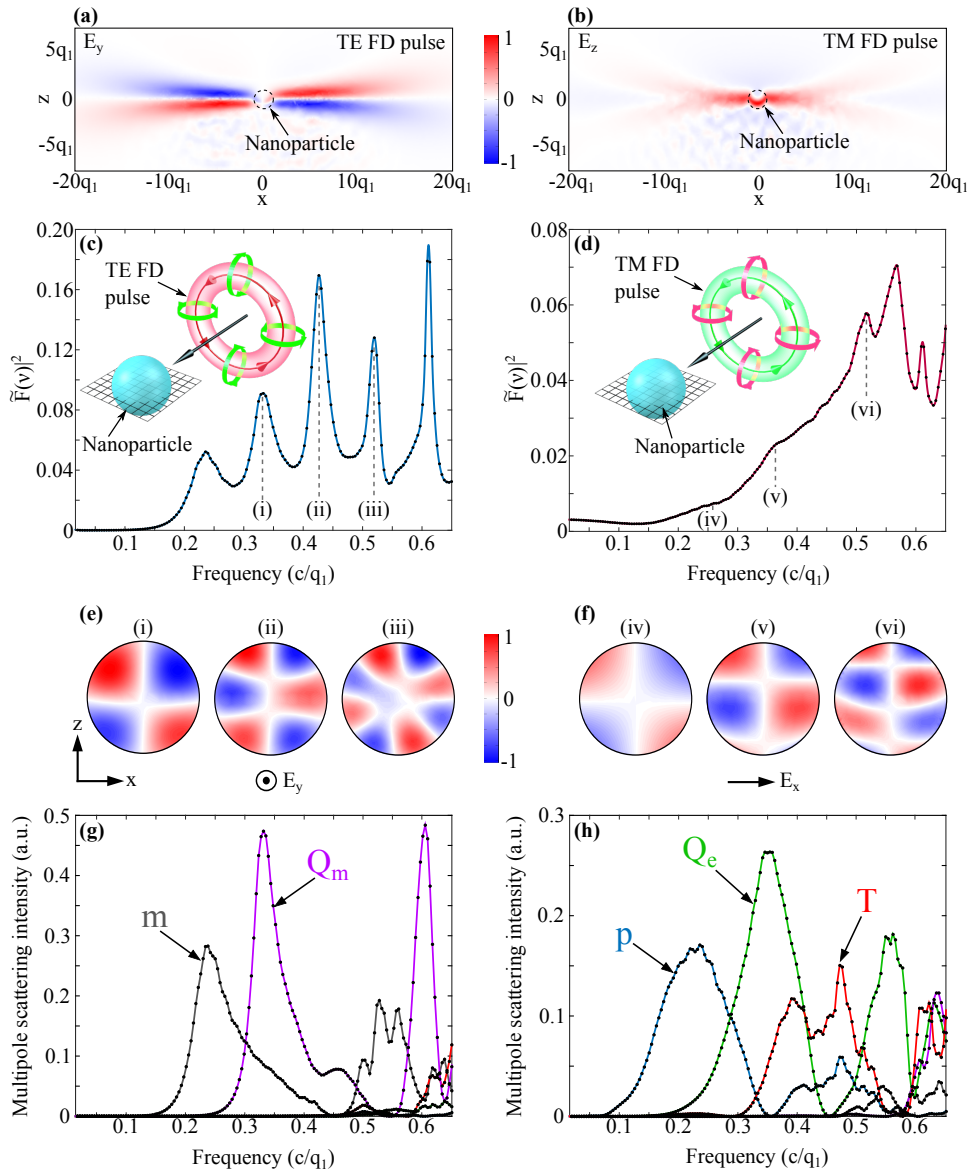


Fig. 6. Interactions of “focused doughnut” pulses with spherical dielectric nanoparticles. (a) and (b) show the xz cross-sections of the COMSOL simulation domain at a time $t = 0$. (a) shows the normalised transverse electric field of a TE FD pulse, and (b) shows the normalised longitudinal electric field of the TM FD pulse. The outline of the spherical nanoparticle is shown by the dotted line. (c) & (d) show the electric field intensity integrated over the volume of the nanoparticle as a function of frequency, when under excitation from a transverse electric (TE) and a transverse magnetic (TM) FD pulse respectively. (e) & (f) show the electric field distributions on an xz cross-section of the nanoparticle (see grid in the insets to (c) & (d)) at resonance positions (i)-(vi). (g) & (h) show the scattering intensity of the individual cartesian multipoles up to quadrupole order (electric dipole p , magnetic dipole m , toroidal dipole T , electric quadrupole Q_e , and magnetic quadrupole Q_m) for illumination with TE and TM FD pulses, respectively. In (c)-(d) & (g)-(h) dots correspond to simulation data points, while lines serve as eye guides.

$$\text{Electric dipole} \quad \mathbf{p} = \frac{1}{i\omega} \int \mathbf{j} d^3 r \quad (5)$$

$$\text{Magnetic dipole} \quad \mathbf{m} = \frac{1}{2c} \int (\mathbf{r} \times \mathbf{j}) d^3 r \quad (6)$$

$$\text{Toroidal dipole} \quad \mathbf{T} = \frac{1}{10c} \int [(\mathbf{r} \cdot \mathbf{j}) \mathbf{r} - 2r^2 \mathbf{j}] d^3 r \quad (7)$$

$$\text{Electric quadrupole} \quad Q_{\alpha\beta}^e = \frac{1}{2i\omega} \int \left[r_\alpha j_\beta + r_\beta j_\alpha - \frac{2}{3} \delta_{\alpha\beta} (\mathbf{r} \cdot \mathbf{j}) \right] d^3 r \quad (8)$$

$$\text{Magnetic quadrupole} \quad Q_{\alpha\beta}^m = \frac{1}{3c} \int [(\mathbf{r} \times \mathbf{j})_\alpha r_\beta + (\mathbf{r} \times \mathbf{j})_\beta r_\alpha] d^3 r \quad (9)$$

Where \mathbf{j} is the induced (polarization) current density. These multipole moments can then be used to calculate the total intensity scattered by the nanoparticle in the far-field:

$$I_{total} = \frac{2\omega^4}{3c^3} |\mathbf{p}|^2 + \frac{2\omega^4}{3c^3} |\mathbf{m}|^2 + \frac{2\omega^6}{3c^5} |\mathbf{T}|^2 + \frac{4\omega^5}{3c^4} (\mathbf{p}^\dagger \cdot \mathbf{T}) + \frac{\omega^6}{5c^5} Q_{\alpha\beta}^e Q_{\alpha\beta}^e + \frac{\omega^6}{20c^5} Q_{\alpha\beta}^m Q_{\alpha\beta}^m \quad (10)$$

Owing to the toroidal topology of the FD pulse, the toroidal family of multipoles are included in this analysis. In recent years, the previously elusive toroidal dipole has been demonstrated as a dominant contributor to the scattering of multiple systems with toroidal topology [22–24]. This includes systems composed entirely of dielectric elements [24]. In contrast, here the incident excitation (the FD) is in possession of toroidal topology, whereas the excited system of the nanoparticle is not. This is particularly relevant for the TM FD pulse, where its azimuthal H and radial and longitudinal E fields are analogous to the poloidal currents and closed loop of magnetic field that compose a toroidal dipole. As such, it is anticipated that a TM FD should excite a non-negligible toroidal dipole within the nanoparticle.

In the case of TE FD incidence on the nanoparticle [Fig. 6(g)] it is clear that the dominant contributors to the scattering are the magnetic multipoles. This is anticipated owing to the azimuthal E field configuration of the TE FD pulse. Contributions from the electric and toroidal multipoles are significantly suppressed. For the case of TM incidence [Fig. 6(h)] however, the multipole excitations are more complex. As expected, electric multipoles dominate at lower frequencies, as a result of coupling to the longitudinal E field of the incident pulse. However at $\sim 0.46(c/q_1)$, the toroidal dipole mode provides the dominant scattering contribution up to quadrupole order. This is a particularly intriguing feature as it demonstrates a significant toroidal response in a system with non-toroidal geometry, reiterating the importance of toroidal multipoles in electrodynamics. It is anticipated that different topologies of nanoparticle interacting with FD pulses could show an even more significant presence of toroidal multipoles.

5. Summary

In conclusion, we have demonstrated that the field configuration of FD pulses, consisting of longitudinal and circulating azimuthal fields, undergoes complex polarisation-sensitive transformations under reflection and refraction at metallic and dielectric interfaces. When FD pulses interact with (non-dispersive) dielectric particles, the single-cycle, broadband nature of the pulse results in the resonant excitation of multiple Mie modes over a wide frequency region. Moreover, the toroidal topology of the pulse allows to excite a prominent toroidal dipole mode in a system of non-toroidal topology. Our results highlight the potential of the FD pulses, especially within the context of the nascent field of toroidal electrodynamics.

Following a period of embargo, the data from this paper can be obtained from the University of Southampton ePrints research repository, DOI: 10.5258/ SOTON/386832.

Acknowledgments

The authors would like to acknowledge the financial support of the Defence Science and Technology Laboratory, the UK's Engineering and Physical Sciences Research Council (grant EP/M008797/1), the Leverhulme Trust, the MOE Singapore (grant MOE2011-T3-1-005) and the Royal Society.